

Radar Extrapolation Scheme

Yadong Wang^{*1}, Jian Zhang²

¹Electrical and Computer Engineering Department,
Southern Illinois University Edwardsville, Edwardsville, IL

²Natioanl Severe Storms Laboratory, Norman, OK

1. Introduction

Very short term (0~3 hours) radar based quantitative precipitation forecasting (QPF), also known as nowcasting, plays an important role in flood warning and other hydrological applications. Three major categories of techniques have been developed during the past half century: conceptual models of convection initiation and dissipation, explicit numerical prediction of thunderstorms, or the extrapolation of the most recent observations (Wilson et al. 1998, Wilson 2003).

Radar based QPF approaches predict storm motions through extrapolating the radar observation patterns into the future. Precipitation motion field, which plays the critical role in radar based QPF, can be derived with either pattern matching approaches or centroid tracking approaches. In pattern matching approaches, the motions of an entire field or its components are established through some forms of cross correlation (e.g. Rinehart and Garvey 1978; Rinehart 1981; Bellon and Austin 1984; Li et al. 1995). The extrapolation using precipitation motion field derived from cross correlation or NWP model winds is considered as the optimum method for nowcasting widespread and persistent rains (Ryall and Conway 1994; Pierce et al. 2004). On the other hand, the centroid tracking approach derives a motion vector through tracking the temporal sequence of observed radar image's centroid positions (e.g. Austin and Bellon 1982; Rosenfeld 1987; Dixon and Wiener 1993, Johnson et. al. 1998, Lakshmanan and Smith 2009). The centroid tracking based nowcasting approaches are well suited to the prediction of convection and its associated severe weather such as damaging winds, hails, tornadoes, and etc., but not well developed for the surface precipitation prediction (Pierce et al. 2004). This work aims at developing and testing a novel radar based QPF approach that combines the centroid tracking approach and the rapid refresh (RAP) model for the

surface precipitation prediction. Moreover, the variations of the precipitation properties, such as the precipitation cell size, total water content, and precipitation intensity are also incorporated into the prediction. This paper is organized as follows. In section 2, the method for the storm tracking and prediction is introduced. The performance of the proposed approach is discussed in section 3, and summary and conclusion are given in section 4.

2. Methodology

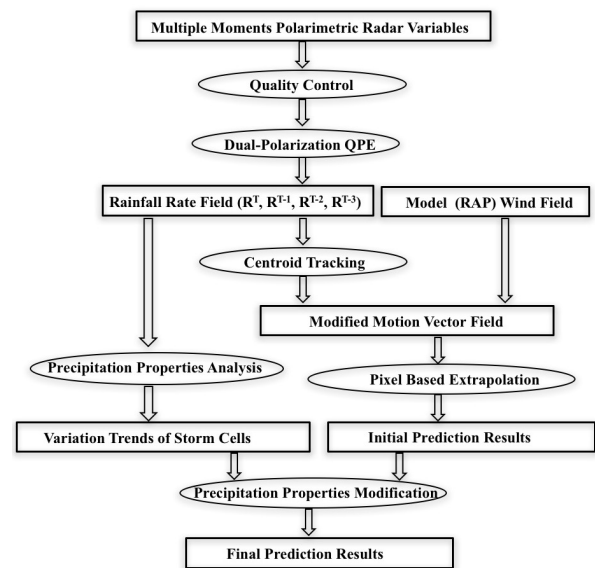


Figure 1. The flow char of the proposed radar based QPF approach.

The flow chart of the proposed radar based QPF approach is shown in Fig. 1. The inputs to the algorithm are the polarimetric radar variables of reflectivity (Z), differential reflectivity (Z_{DR}), and differential phase (ϕ_{DP}) from four continuous moments (T , $T-1$, $T-2$ and $T-3$). The time interval of this work is 10 minutes. The wind field from the Rapid Refresh (RAP), an hourly

**Corresponding author address: Yadong Wang, Electrical and Computer Engineering Department, Southern Illinois University Edwardsville, Edwardsville, IL.
e-mail: yadwang@siue.edu*

updated assimilation and model forecast system operated by National Centers for Environmental Prediction (NCEP), is another input to this algorithm. The output is the predicted rainfall rate in the unit of mm hr^{-1} .

The radar data is first processed with a physically based radar data quality control approach to eliminate the interference from clutters and other nonprecipitation radar echo (Tang et al. 2014). The processed radar data (Z , Z_{DR} , and K_{DP}) is then used to estimate the rainfall rate based on the hydrometeors classification result (Giangrande and Ryzhkov, 2008). An example of the reflectivity before (A) and after (B) quality control procedure, and estimated rainfall rate (C) is shown in Fig. 2.

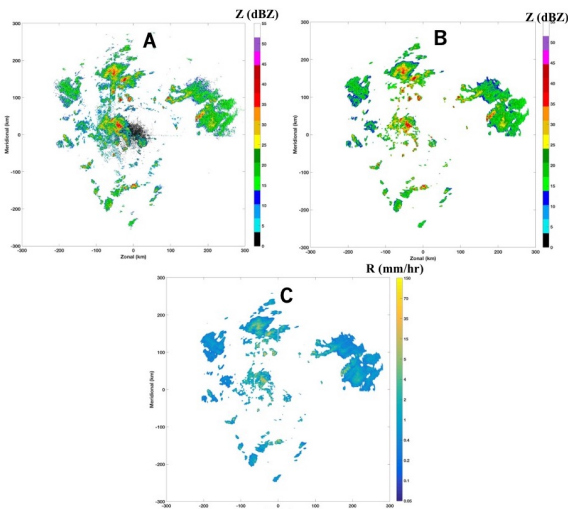


Figure 2. The raw reflectivity (A), quality controlled reflectivity (B), estimated rainfall rate (C).

The obtained rainfall rates from individual radar are then mosaicked using the approach proposed by Zhang et al. (2016). An example of the mosaicked rainfall rate is shown in Fig. 3. In this example, the rainfall rate from 17 radars in Texas and Oklahoma are mosaicked, which covers the area of: 25 N ~ 40 N in latitude, and 110 ~ 90 W in longitude. The spatial and temporal resolution for the mosaicked rainfall rate is 1 km-by-1 km, and 10 minutes, respectively.

2.1 Precipitation motion field derivation

2.1.1 Motion field from centroid tracking

An approach similar to TITAN (Dixon and Wiener 1993) is used in this work to derive the initial precipitation motion field. In this approach, the mosaicked rainfall rate field is first segmented into storm "cells" using threshold of 0 mm hr^{-1} as shown in Fig. 4, where red and black lines are used to indicate the rainfall rate contours ($> 0 \text{ mm hr}^{-1}$) at current and previous (10 minutes earlier) moments, respectively. In this example, a big storm cell can be found in the center of

the area, and small cells can be found on the right side. Since the time interval between these two moments are 10 minutes, the movements of relative big cell are not easily identified because of shape variations.

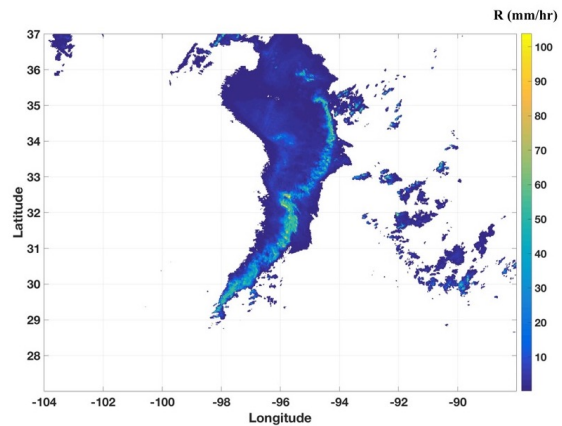


Figure 3. The rainfall rate mosaic at 2210 UTC 25 May 2015.

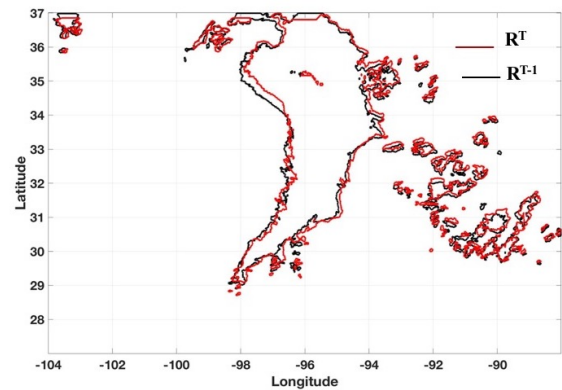


Figure 4. The contours of segmentations at 2210 UTC (red) and 2200 UTC (black) 25 May 2015.

The center of each cell is then calculated with a K-mean method (e.g. Spath 1985; Arthur and Vassilivskii 2007) as shown in Fig. 5. Matching storm cells at $T-1$ and their counterparts at T using an approach similar to the one proposed by Dixon and Wiener (1993). The correct matching pair in Fig. 5 (e.g. C_1^{T-1} and C_1^T) associates with short distance, similar characteristics (size, and total water content), and within the maximum travel distance (Dixon and Wiener 1993). Suppose there are total n_1 and n_2 cells are identified from $T-1$ and T . For the i^{th} cell (center at (x_i^T, y_i^T)) at $T-1$, there are n_2 possible counterparts at T . The distance, size, and total water content is calculated as:

$$d_{i,j} = \left[(x_i^T - x_j^{T-1})^2 + (y_i^T - y_j^{T-1})^2 \right]^{1/2} \quad (1)$$

$$s_{i,j} = \left[(V_i^T - V_j^{T-1})^2 \right]^{1/2} \quad (2)$$

$$t_{i,j} = \left[(\sum R_i^T - \sum R_j^{T-1})^2 \right]^{1/2} \quad (3)$$

where $j = 1, \dots, n_2$, V_i and R_i are the total pixel number and the rainfall rate from i^{th} cell, respectively. Different from Dixon and Wiener (1993), which finds the matching pairs through solving cost function using Hungarian method, the matched pair is identified through minimizing the normalized summation of these three factors.

$$C_{i,j} = w_1 \frac{d_{i,j}}{\max(d)} + w_2 \frac{s_{i,j}}{\max(s)} + w_3 \frac{t_{i,j}}{\max(t)} \quad (4)$$

where $w_1 = w_2 = w_3 = 1$. The maximum travel distance is set as 20 km given the 10 minutes interval between $T-1$ and T . The precipitation motion vector is then calculated using the centroids shift as shown in Fig. 5.

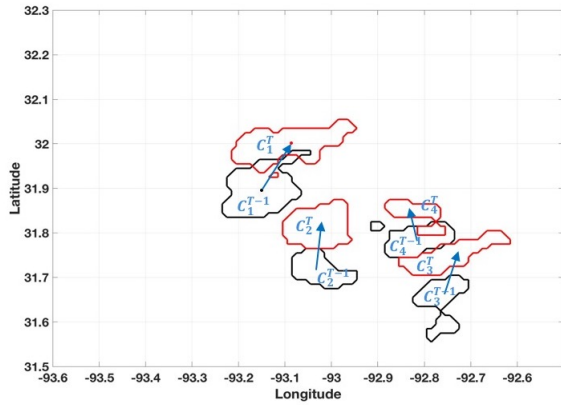


Figure 5. Motion vectors from three cells (C_1 , C_2 , C_3 , and C_4).

2.1.2 Motion field from RAP model

The Rapid Refresh, an hourly updated assimilation and model forecast system, was implemented as an operational forecast system at the NOAA/National Centers for Environmental Prediction (NCEP) in 2012 (Stanley et al. 2016). The RAP model can produce horizontal wind components (U and V) in spatial resolution of 10 km and temporal resolution of 1 hour. An example of the RAP model wind field from 850 hPa layer at 2200 UTC 05/25/2015 is shown in Fig. 6 (A), and the field from the same area as from Fig. 5 is shown in Fig. 6 (B). Four cells are also included as references. It could be found that both the direction and magnitude of the wind field (U and V) calculated from the centroid tracking and the model are different for all of these four cells. In this work, the RAP model wind field is interpolated into 1 km-by-1 km spatial resolution for the purpose of combining with centroid tracking results.

2.1.3 Combination of tracking and model wind field

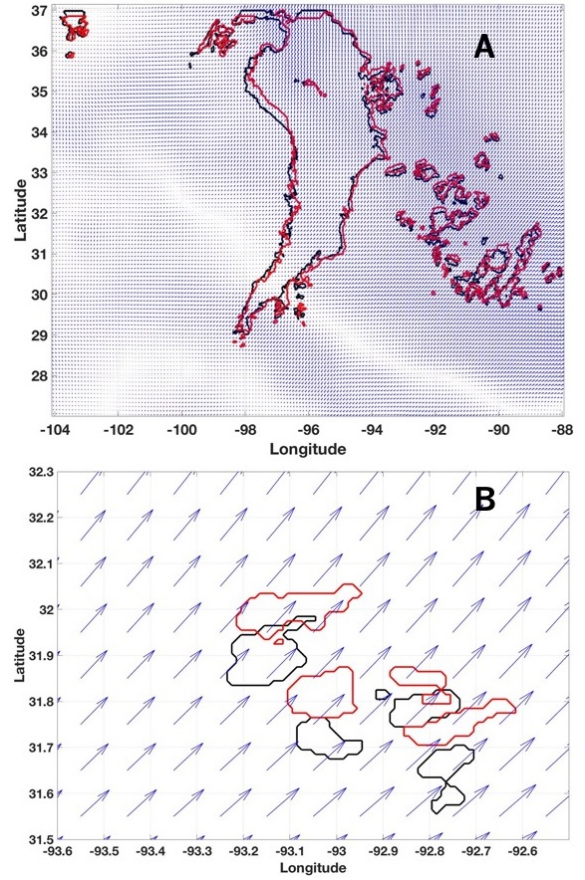


Figure 6. The model wind field at 2200 UTC 05/25/2015

In the centroid tracking approach, such as TITAN (Dixon and Wiener 1993), one velocity (U and V) is assigned to one cell, and all pixels within this cell is assumed moving with the same velocity. For small area cells, the single velocity may represent the whole cell movement. However, for a large area cell, single velocity is not enough to capture the whole cell movement. Since the model field can provide the velocity distribution within a cell, combine the velocity field from centroid tracking and model is an optimal solution. In this work, the velocity from model field is corrected as:

$$U_{i,j} = U_{i,j}^{model} + (\langle U_i^{model} \rangle - U_i^{tracking}) \quad (5)$$

$$V_{i,j} = V_{i,j}^{model} + (\langle V_i^{model} \rangle - V_i^{tracking}) \quad (6)$$

where U^{model} (V^{model}) and $U^{tracking}$ ($V^{tracking}$) are velocity from model and tracking, subscripts " j " and " i " indicate the j^{th} pixel in the i^{th} cell, and " $\langle \rangle$ " is mean operation. An example of the model (blue), and the

corrected final (red color) wind velocity from one cell is shown in Fig. 7.

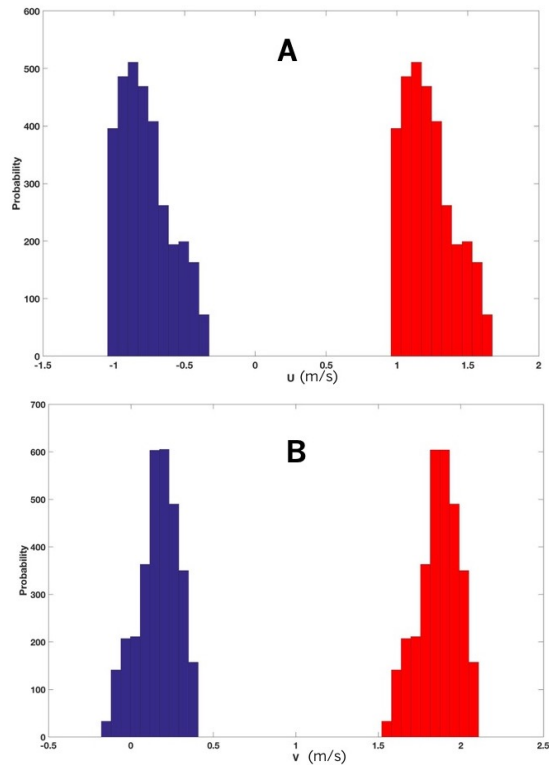


Figure 7. Example of velocity distribution from model (blue) and corrected (red) wind velocity.

2.2 Precipitation properties analysis

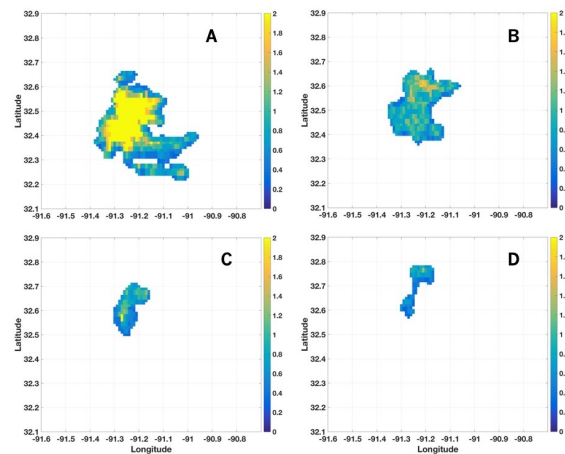


Figure 8. One precipitation cell at T-3 (A), T-2 (B), T-1 (C), and T (D).

The evaluation of one cell at T-3, T-2, T-1 and T is shown in Fig. 8. It could be found from this example that not only the size shrinks from T-3 to T, but the total

water content continuously decreases, and high intensity pixels disappears. Three variables are defined in this work to quantify the precipitation cell properties:

- Size: the total number of pixels in one cell with value larger than 0 mm hr^{-1} .
- Total water content: the summation of all the pixels in one cell.
- Pixel number at each Intensity level: number of pixels in each intensity level. In this work, the intensity level interval is 1 mm hr^{-1} .

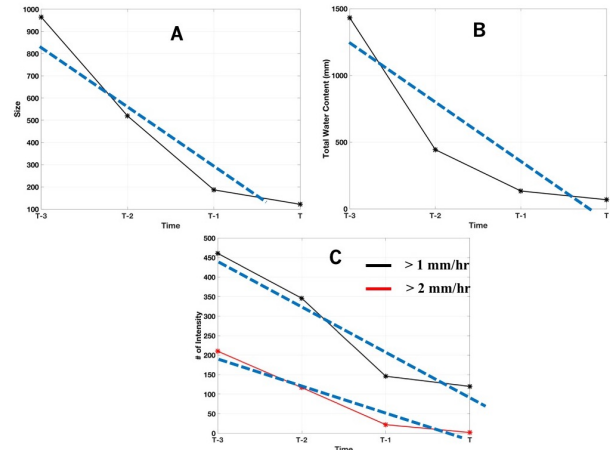


Figure 9. Trend of the precipitation properties: (A) size, (B) total water content, and (C) number of pixels at each intensity level.

2.3 Prediction

After the precipitation motion field is obtained through the combination of centroid tracking and model wind field, the initial prediction result is calculated through the pixel-based linear extrapolation as proposed by Dixon and Wiener (1993). The trend of precipitation properties (size, water content, and # intensity level) are linearly fitted as shown in Fig. 9 with dashed line. The initial prediction is adjusted according to the trend of the precipitation properties.

3. Performance Evaluation

The performance of proposed approach is evaluated using the flash flood case in Taxes and Oklahoma on 25 May 2015. The mosaicked rainfall rate at 2200 UTC and 2300 UTC is shown in Fig. 9 (A) and (B), and the predicted rainfall rate at 2300 UTC is shown in Fig. 9 (C). Four approaches are evaluated in the current work: I.) prediction using the motion field derived from centroid tracking approach only; II) prediction using the motion field from model field only; III) prediction using motion field from the combination of centroid tracking and model field, but without precipitation properties adjustment; and IV) same as III but with precipitation properties adjustment.

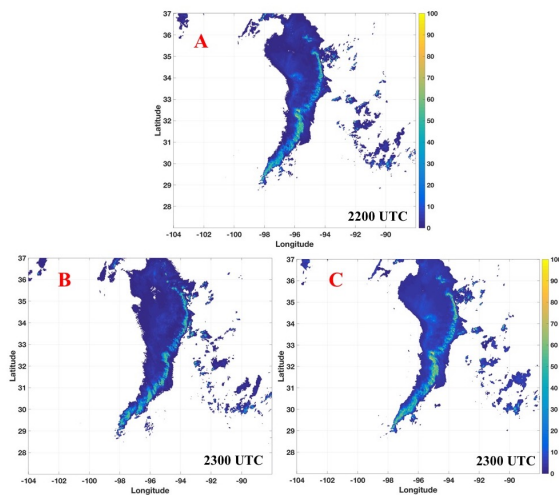


Figure 9. (A) QPE results at 2200 UTC, (B) QPE results at 2300 UTC, and (C) prediction results at 2300 UTC.

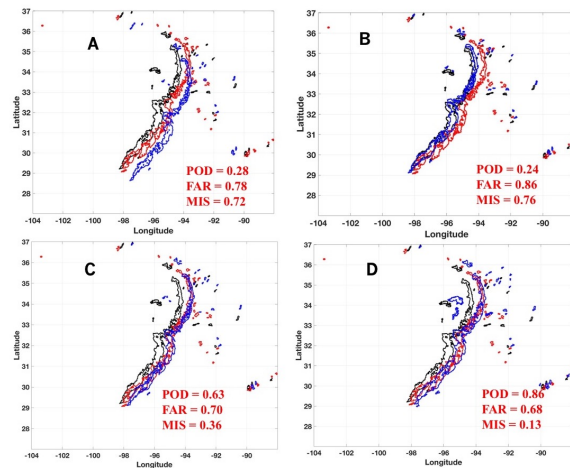


Figure 10. (A) result from centroid tracking only; (B) result from model field only; (C) result from combination of centroid tracking and model field, without precipitation properties adjustment; (D) similar to III but with precipitation properties adjustment.

The contours of rainfall rate above 10 mm hr^{-1} from QPE and prediction results are shown in Fig. 10, where the black, red, and blue lines are used to indicate the contours from QPE at 2200 UTC, QPE at 2300 UTC, and prediction at 2300 UTC, respectively. The QPE at 2300 UTC is defined as “ground truth”. Three scores are used to evaluate the performance: 1.) $POD = a/(a+c)$, 2.) $FAR = b/(a+b)$, 3.) $MIS = c/(a+c)$, where a , b , and c represent “hit”, “false”, and “miss”. The term “hit” is defined as prediction and ground truth both above 10 mm hr^{-1} , and “false” and “miss” is only prediction and ground truth above 10 mm hr^{-1} , respectively. The scores for each approach are

presented in each figure. It could be found that using tracking or model field only can't fully capture the storm cells movement, and the combination can have much better performance. The precipitation properties adjustment can further enhance the accuracy.

5. Summary

A quantitative precipitation forecasting (QPF) approach combining centroid tracking and RAP model wind field is developed and tested in the current work. The analysis of precipitation properties is also introduced to further enhance the accuracy of the proposed QPF approach. Comparing with the QPF approaches rely on centroid tracking only, model field only, and the approach without precipitation properties analysis, the proposed new approach produce the optimal results with highest probability of detection (POD), lowest false alarm rate (FAR) and miss detection.

6. References

- Arthur, David, and Sergi Vassilvitskii. “K-means++: The Advantages of Careful Seeding.” *SODA '07: Proceedings of the Eighteenth Annual ACM-SIAM Symposium on Discrete Algorithms*. 2007, pp. 1027–1035.
- Austin, G. L., and A. Bellon, 1982: Very short range forecasting of precipitation by objective extrapolation of radar and satellite data. Nowcasting, K. Browning, Ed., Academic Press, 177-190
- Bellon, A., and G. L. Austin, 1984: The accuracy of short-term rainfall forecasts. *J. Hydrol.*, **70**, 35-49.
- Dixon, M. and G. Weiner, 1993: TITAN: Thunderstorm Identification, Tracking Analysis and Nowcasting - A radar-based methodology. *J. Atmos. Oceanic Technol.*, **10**, 785-797
- Giangrande, S., and A. Ryzhkov, 2008: Estimation of rainfall based on the results of polarimetric echo classification. *J. Appl. Meteor.*, **47**, 2445-2462.
- Johnson J. T., P. L. Mackeen, A. Witt, D. Mitchell, G. J. Stumpf, M. D. Eilts, and K. W. Thomas, 1998: The storm cell identification and tracking algorithm: an enhanced WSR-88D algorithm. *Wea. Forecasting*, **13**, 263-276
- Lakshmanan V., and T. Smith, 2010: An objective method of evaluating and devising storm-tracking algorithms. *Wea. Forecasting*, **25**, 701-709
- Li, L., W. Schmid, and J. Joss, 1995: Nowcasting of motion of precipitation with radar over complex terrain.

J. Appl. Meteor., **34**, 1286-1298.

Pierce, C. E., E. Ebert, A. W. Seed, M. Sleigh, C. G. Collier, N. I. Fox, N. Donaldson, J. W. Wilson, R. Roberts, C. K. Mueller, 2004: The nowcasting of precipitation during Sydney 2000: an appraisal of the QPF algorithm. *Wea. Forecasting*, **21**, 7-21.

Rinehart, R. E., 1981: A pattern recognition technique for use with conventional weather radar to determine internal storm motions. *Atmos. Technol.*, **13**, 119-134.

Rinehart, R. E., and E. E. Garvey, 1978: Three dimensional storm motion detection by conventional weather radar, *Nature*, **273**, 287-289.

Rosenfeld D., 1987: Objective method for analysis and tracking of convective cells as seen by radar. *J. Atmos. Oceanic Technol.*, **4**, 422-434.

Ryall, G. and B. W. Conway, 1994: Automated precipitation nowcasting at the UK Met Office. Preprints, *First European Conf. on Applications of Meteorology*, Oxford, United Kingdom, University of Oxford.

Spath, H. *Cluster Dissection and Analysis: Theory, FORTRAN Programs, Examples*. Translated by J. Goldschmidt. New York: Halsted Press, 1985.

Stanley G. B., and coauthors, 2016: A north American hourly assimilation and model forecast cycle: the rapid refresh. *Mon. Wea. Rev.*, **144**, 1669-1694

Tang, L., J. Zhang, C. Langston, J. Krause, K. Howard, and V. Lakshmanan, 2014: A physically based precipitation-nonprecipitation radar echo classifier using polarimetric and environmental data in a real-time national system. *Wea. Forecasting*, **29**, 1106-1118

Wilson, J., 2003: Thunderstorm nowcasting: Past, present and future, Preprints, *31st Conf. on Radar Meteorology*, Seattle, WA, Amer. Meteor. Soc., J13-19.

Wilson, J., N. A. Crook, C. K. Mueller, J. Sun, and M. Dixon, 1998: Nowcasting thunderstorms: A status report. *Bull. Amer. Meteor. Soc.*, **79**, 2079-2099.

Zhang, J., and Coauthors, 2016: Multi-radar multi-sensor (MRMS) quantitative precipitation estimation: initial operating capabilities. *Bull. Amer. Meteor. Soc.*, **97**, 621-638, doi:10.1175/BAMS-D-14-00174.1